12th International Conference on Fracture Mechanics of Concrete and Concrete Structures
FraMCoS-12
B.L.A. Pichler, Ch. Hellmich, P. Preinstorfer (Eds)

https://doi.org/10.21012/FC12.1329
MS09-1:4

ANALYSIS OF TEMPERATURE-INDUCED DEGRADATION IN THE FRACTURE BEHAVIOR OF POLYOLEFIN FIBER-REINFORCED SELF-COMPACTING CONCRETE

P. MAZÓN[*], A. ENFEDAQUE[*], A. PICAZO[†], M.G. ALBERTI[*] AND J.C. GÁLVEZ[*]

[*] Departamento de Ingeniería Civil: Construcción, E.T.S de Ingenieros de Caminos, Canales y Puertos, Universidad Politécnica de Madrid. C / Profesor Aranguren, 3, 28040, Madrid, Spain
e-mail: pablo.mazon.ortiz@upm.es; alejandro.enfedaque@upm.es; marcos.garcia@upm.es; jaime.galvez@upm.es

[†] Departamento de Tecnología de la Edificación, E.T.S de Edificación, Universidad Politécnica de Madrid. Avda. Juan de Herrera, 6, 28040, Madrid, Spain
e-mail: a.picazo@upm.es

Key words: High temperature, flexural tensile strength, fracture behaviour, polyolefin fibres, fibre reinforced concrete.

Abstract: Concrete has been the most widely used construction material in recent decades, while the use of macro-polymer fibres has gained increasing attention due to their significant advantages. Despite the commendable structural performance of concrete, it is crucial to recognize that fiber-reinforced concrete faces a substantial risk when exposed to certain conditions, such as elevated temperatures. Although there is extensive scientific literature on this subject, much of it does not capture the material's behaviour at the precise moment it is subjected to high temperatures. To address this gap, the present research focuses on analysing the flexural response of fiber-reinforced concrete at 20°C, 165°C, 185°C, and 200°C. For this study, it was essential to carefully isolate the specimens to minimize temperature loss during testing. Upon completion of the tests and thorough fracture surface analysis, the results indicated that polyolefin fibers reduce the risk of spalling; as temperature increases, the residual load-bearing capacity of the material diminishes, approaching that of plain concrete at the highest temperature studied.

1 INTRODUCTION

Concrete is a widely used construction material, but its cement production significantly contributes to global CO_2 emissions. Enhancing durability is crucial to mitigate its environmental impact, as durability reduces crack formation and ingress of harmful substances [1-3].

Fiber-reinforced concrete (FRC) improves crack control and mechanical properties. Polymer fiber-reinforced concrete (PFRC) offers chemical stability and structural performance, making it suitable for applications like shotcrete in tunnels [4-9].

This study focuses on the behaviour of PFRC under high temperatures, evaluating fracture properties during heating [10-14]. Specimens with polyolefin fibres were tested at up to 200°C using three-point bending tests, alongside a fracture surface analysis to assess fibre distribution.

The findings enhance understanding of PFRC's performance under extreme conditions, contributing to safer structural designs and reduced environmental impact.

2 SPECIMEN MANUFACTURING

The concrete was produced using Portland cement (EN 197-1 CEM I 52.5 R-SR 5), tap water, and a polycarboxylate-based super-plasticizer (Sika Viscocrete H-20). Aggregates included siliceous gravels (4–8 mm and 4–12 mm, max. size 12.7 mm) and 0–2 mm sand. A limestone powder with >98% calcium carbonate content and a specific gravity of 2700 kg/m³ was added to increase fine particles. The mix formulation, labeled P0, is summarized in Table 1.

Table 1. Concrete formulations in kg/m³.

Material	P10	P0
Cement CEM I 52.5 R-SR 5	375	375
Limestone powder	200	200
Water (0.5 w/c)	187.5	187.5
Gravel	367	367
Grit	245	245
Sand	918	918
Superplasticizer (% cement weight)	1.35	1.00
48 mm Polyolefin fibres	10	0

P10 incorporated 10 kg/m³ of 48 mm polyolefin fibers with an embossed, surface-treated finish to enhance fiber-matrix adhesion. Key properties of the fibers are listed in Table 2.

Table 2. Relevant properties of the fibers.

Property	48 mm fiber
Density (kg/cm³)	0.91
Equivalent diameter (mm)	0.84
Length (mm)	48
Tensile strength (MPa)	465–530
Modulus of elasticity (GPa)	8.8
Melting point (°C)	164

Concrete mixes (P0 and P10) were prepared in a 100 liters planetary mixer and tested in the fresh state as per EN 12350-8:2010, confirming their self-compacting properties (Table 3).

Table 3. Fresh state properties.

Parameter	P10	P0
T50 (s)	6.0	3.5
df (mm)	590	650

Specimens were cast, including prismatic (600x150x150 mm³) and cylindrical (ø150x300 mm³) shapes. Prisms included thermocouples for temperature monitoring during heating and testing, as shown in Figure 1. After 24 hours, specimens were demolded and cured at 20±2°C and >95% relative humidity. At 28 days, compressive strengths were 61.4 MPa (P0) and 67.6 MPa (P10), following EN 12390-3.

Twin notches were introduced near thermocouple positions before heating to analyze thermal conductivity effects.

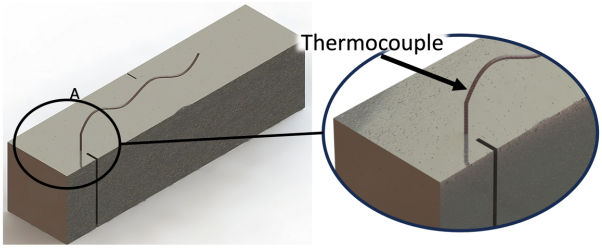

Figure 1. Position of the thermocouple.

3 EXPERIMENTAL CAMPAIGN

During the fracture tests, specimens were insulated to maintain the target temperature. They were coated with 30 mm mineral wool panels with an aluminium layer, offering a thermal conductivity of 0.035 W/m·°K. The notches were filled with rock wool to minimize temperature loss near the ligament.

Specimens were heated in a Hobersal XB7/115 DS PAD furnace, capable of reaching 1150°C, with controlled heating profiles. Temperature monitoring was performed using thermocouples connected to an HBM data acquisition system. The heating process lasted 24 hours to ensure thermal stability, with target temperatures set at 165, 185, and 200°C, corresponding to the melting point of polyolefin fibers (164°C).

Fracture tests followed standard room-temperature procedures, using an Instron 8803 servo-controlled universal machine (500 kN). A CMOD device measured notch opening, while two LVDTs recorded mid-span deflection. Data collected included load, notch opening, deflection, and synchronized specimen temperature (Fig. 2). Tests continued

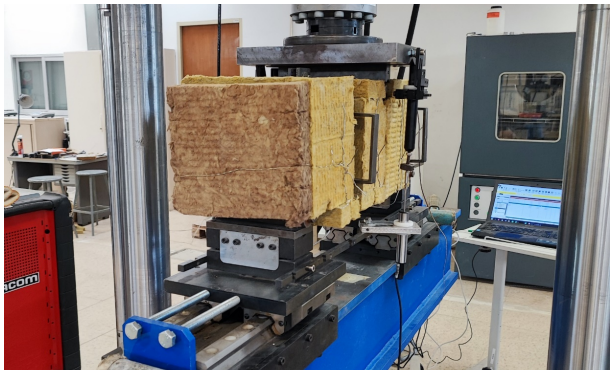

Figure 2. Test specimen equipped with measurement systems.

until the deflection exceeded 10 mm, when the CMOD reached its measurement limit.

4 TEST RESULTS AND DISCUSSION

The experimental campaign evaluated the impact of temperature on fiber-reinforced concrete through two primary aspects: mechanical performance in three-point bending fracture tests and fracture surface analysis.

4.1 Flexural tensile tests

The flexural tensile tests followed the EN-14651:2007 standard [15] on notched prismatic specimens to evaluate the degradation of fiber-reinforced concrete mechanical properties with temperature. The key objective was to determine whether the fibers maintain structural relevance at elevated temperatures, by EN 14889-2:2008 [16] and Model Code 2010 (MC2010) [17].

According to MC2010, fibers can contribute to structural design if $f_{R1}/f_{LOP} > 0.4$ and $f_{R3}/f_{R1} > 0.5$, where f_{LOP} represents the proportionality limit strength, and f_{R1} and f_{R3} are residual strengths at 0.5 mm and 2.5 mm CMOD, respectively. Additionally, EN14889-2:2008 requires $f_{R1} > 1.5$ MPa and $f_{R4} > 1.0$ MPa (where f_{R4} is the residual strength at 3.5 mm CMOD).

The experimental campaign examined the effect of temperature on polyolefin fiber-reinforced concrete. Results showed a decline in residual strength with increasing temperature, affecting compliance with structural criteria. Figure 3 compares unreinforced concrete specimens (P0) and fiber-reinforced specimens (P10), tested at

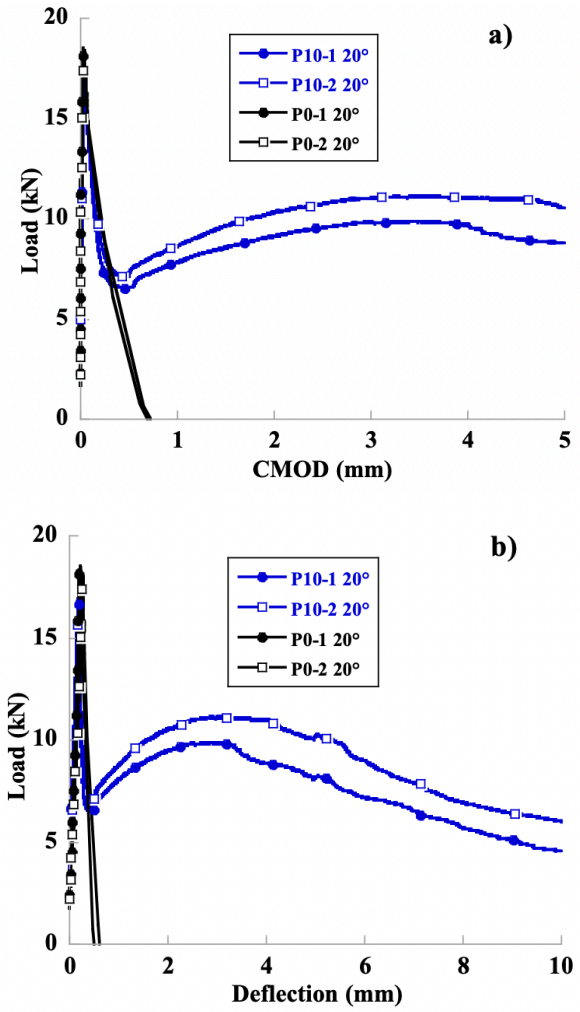

Figure 3. a) Load-CMOD curves and b) Load-deflection curves of P0 and P10, tested at room temperature.

room temperature, highlighting baseline performance before thermal exposure.

The plain concrete specimens (P0) exhibited a sharp reduction in load-bearing capacity after reaching a peak load of ~18 kN, showing brittle failure due to the lack of reinforcement, consistent with previous studies [18].

In contrast, polyolefin fiber-reinforced specimens (P10) displayed the typical three-stage behaviour [19,20]. After reaching a peak load of ~16 kN, the load gradually decreased to an inflection point at ~6.75 kN, followed by a reloading phase driven by fiber contribution. At 20°C, the maximum loads during this stage were 11.21 kN and 9.93 kN for the two tested beams.

Figure 4 presents the response of P10 specimens subjected to 165°C and 185°C, temperatures chosen based on the fibre melting

point (164°C, per manufacturer data). Despite initially following a similar trend as room-temperature tests, the heating process weak-

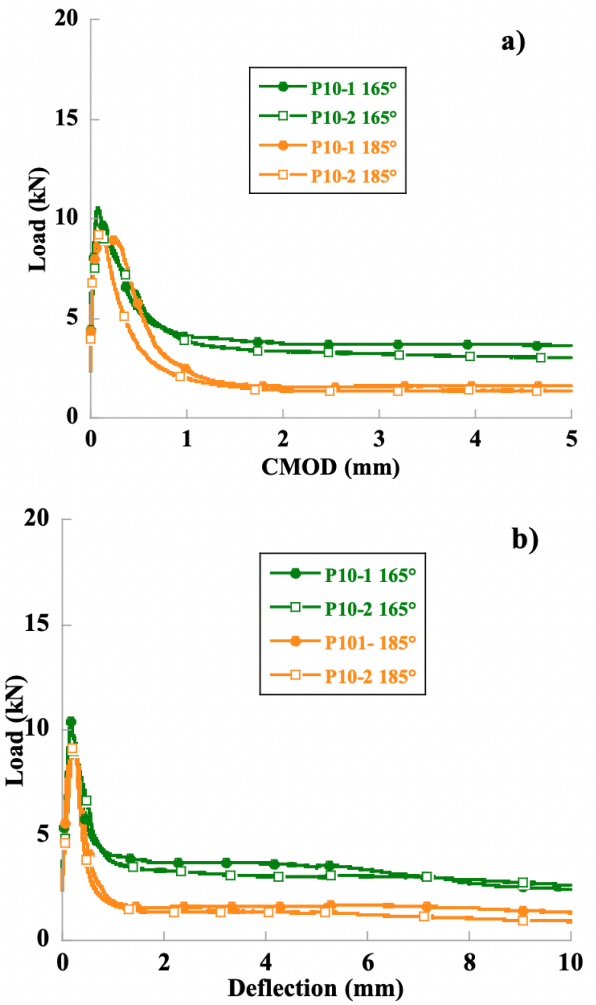

Figure 4. a) Load-CMOD curves and b) Load-deflection curves of P10, tested at 165 and 185°C.

ened the concrete matrix, leading to 37.6% and 45.1% reductions in peak load at 165°C and 185°C, respectively, compared with P10 at 20°C.

Given the melting point of polyolefin fibers, the concrete was expected to behave as unreinforced. However, Figure 4 shows this assumption is inaccurate. Although no clear reloading stage is observed, no sudden load drop occurred. The residual load-bearing capacity stabilized around 4.10 kN at 165°C and 1.88 kN at 185°C. Beyond this, the reduction remained gradual. Notably, at a CMOD of 2.5 mm, the load at 165°C (3.70 kN) was higher than at 185°C (1.41 kN), representing a 61.9% reduction.

Figure 5 compares P10 at 20°C and 200°C, where the latter behaves similarly to plain concrete. The initial load-bearing stage remains

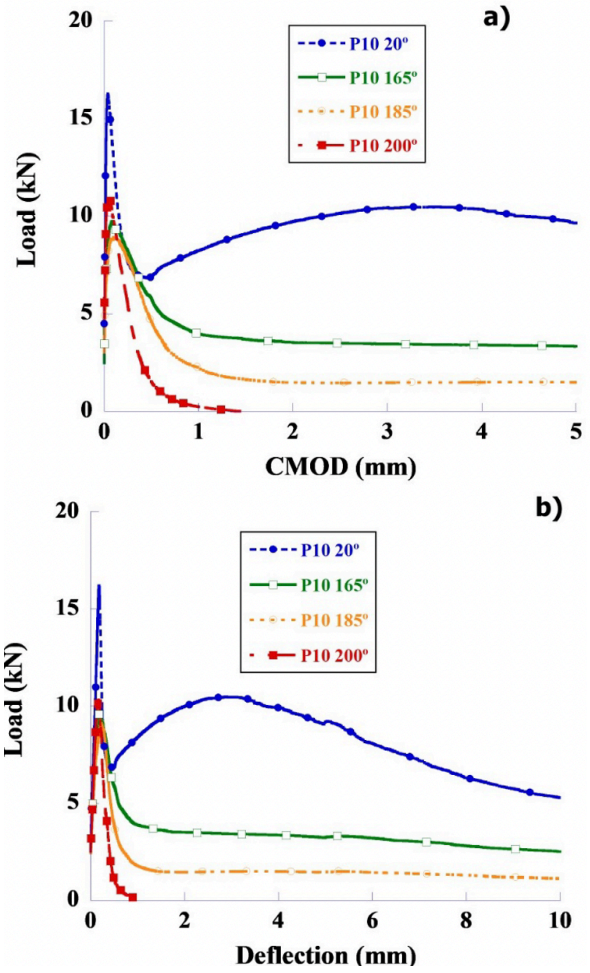

Figure 5. a) Load-CMOD curves and b) Load-deflection curves of P10, tested at 20ºC and 200ºC.

linear, governed by the matrix properties. At 20°C, P10 reached 16.92 kN, whereas at 200°C, it dropped to 11.40 kN, a 32.6% reduction.

For P10 at 200°C, after reaching peak load, a sharp decline in load-bearing capacity occurred. However, unlike unreinforced concrete, it retained a residual load of 0.94 kN, as seen in Figure 5.

To analyze the effect of temperature on P10, Figure 6 presents the average behavior at 20°C, 165°C, 185°C, and 200°C, highlighting the progressive reduction in strength. Notably, low scatter was observed among tests conducted at the same temperature, reinforcing the consistency of the results.

P10 exhibited an initial linear load branch across all tested temperatures, governed by the concrete matrix. However, temperature significantly affected load-bearing capacity, with peak loads decreasing from 16.27 kN at 20°C to 9.74 kN at 165°C, 8.90 kN at 185°C, and 10.94 kN at 200°C, corresponding to reductions of 40.1%, 45.3%, and 32.8%, respectively.

At 20°C, P10 showed reloading behavior, sustaining 10.50 kN after peak load. At 165°C, the unloading slope was similar to 20°C but lacked reloading, stabilizing at 4.1 kN. The 185°C tests displayed a steeper decline, with load stabilizing at 1.88 kN. At 200°C, P10 behaved similarly to plain concrete, indicating a loss of fibre reinforcement effects.

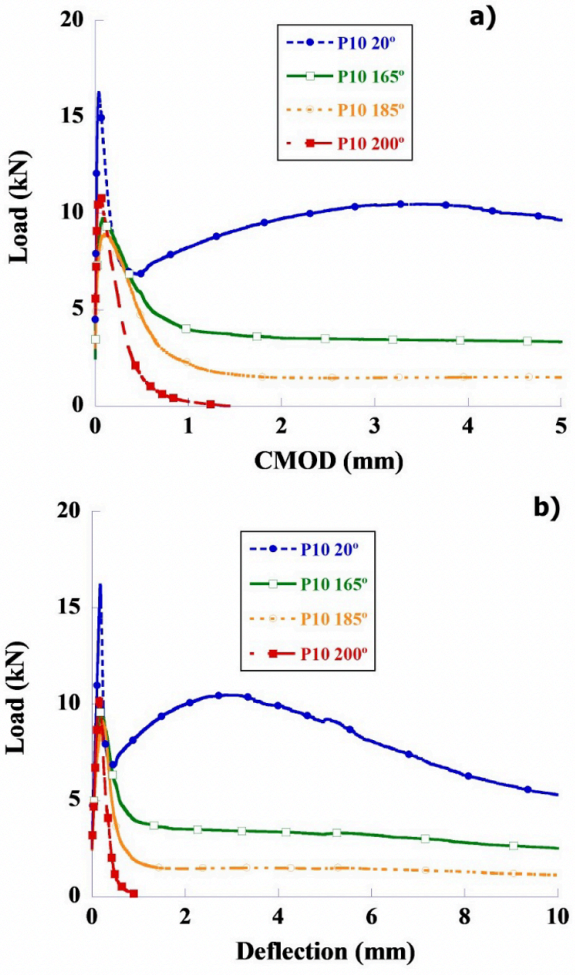

Figure 6. Average curves of P10, tested at 20°C, 165°C, 185°C, and 200°C. a) Load-CMOD and b) Load-deflection

While [21] reported that polymer fibres remained intact below 300°C, the present study shows polyolefin fibres (melting at 164°C) lost significant structural integrity at 185°C and exhibited a drastic reduction at 200°C, confirmed by surface analyses in Section 4.2.

Notably, no spalling was observed in P0 or P10 at any temperature, possibly due to the heating rate and dwell time, differing from findings in [21].

4.2 Fracture surface analysis

The initial load branch is controlled by the concrete matrix strength until reaching peak load, followed by a sharp drop and, in most cases, a secondary load increase, except at 200°C, where this reloading is absent. This increase depends on fibre orientation, distribution, and fibre-matrix interface properties, which influence residual strengths.

At high temperatures, fibre melting or surface deterioration can affect the mechanical bond with the matrix. To assess their contribution to residual flexural tensile strength, a detailed fibre count was conducted in sectors [20], enabling the determination of an orientation coefficient (Equation 1). Figures 7–10 present general and detailed views of tested half-specimens, highlighting these effects.

$$\theta = \frac{n \cdot A_f}{V_f \cdot A} \tag{1}$$

where n is the number of fibres counted in the ligament section, Af is the area of a single fibre section, Vf is the volume of fibres, and A is the area of the ligament.

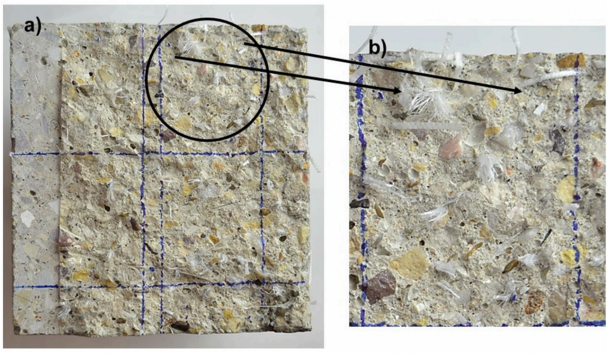

Figure 7. P10 at 20°C half-specimen: a) general section and b) detail.

Figure 7 reveals two categories of fibres on the specimen surface: undamaged fibres and

deteriorated fibres. The latter show fragmentation into smaller filaments (Figure 7b), likely due to fibre pullout following matrix failure. This degradation highlights the negative impact of elevated temperatures on fibre integrity and, consequently, on the mechanical performance of fibre-reinforced concrete.

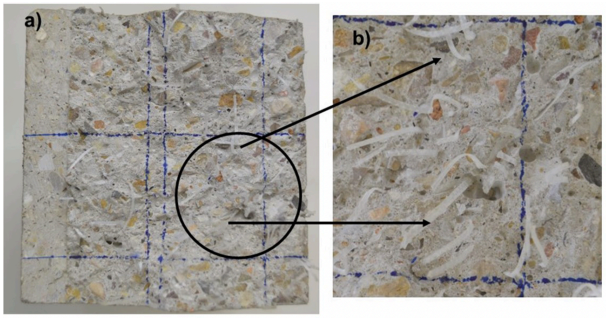

Figure 8. P10 at 165°C half-specimen: a) general section and b) detail.

With increasing temperature, the polyolefin fibres' performance deteriorated, despite their melting point being 164°C. At 165°C, fibres remained visible (Figure 8) but lost surface roughness, reducing adhesion to the matrix. This led to a decrease in L_{MIN} and L_{REM} values compared with specimens tested at room temperature, indicating a weakened mechanical contribution.

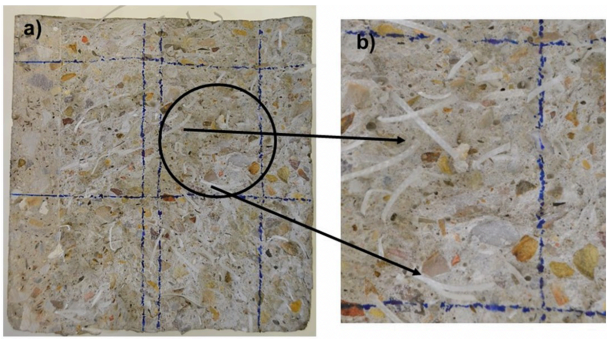

Figure 9. P10 at 185°C half-specimen: a) general section and b) detail.

Figure 9 shows a behaviour similar to that observed at 165°C, where the fibres experienced a loss of roughness. At the end of the test at 185°C, it was found that the fibres had a soft texture and could be separated with minimal effort from the matrix. This phenomenon could explain the lower values of L_{MIN} and L_{REM} compared with those obtained in the tests conducted at 165°C.

Figures 8 and 9 show minimal differences in fracture surfaces, with no significant changes in fibre morphology despite temperature variations. However, Figure 10 reveals notably shorter fibres compared with Figures 7–9. This length reduction, consistent with previous studies [22], may contribute to the decline in mechanical properties observed at higher temperatures.

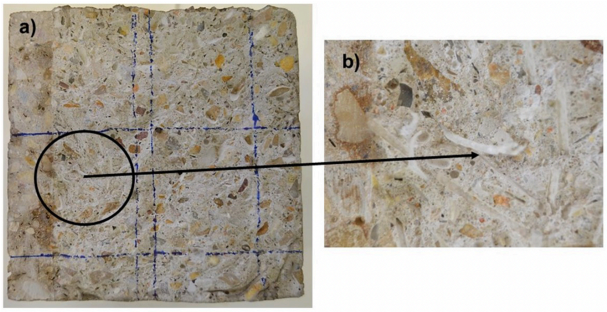

Figure 10. P10 at 200°C half-specimen: a) general section and b) detail.

Table 4. Number of fibres counted in the specimens.

Specimens	Fiber count
P10-1 20°C	211
P10-2 20°C	229
P10-1 165°C	268
P10-2 165°C	250
P10-1 185°C	220
P10-2 185°C	201
P10-1 200°C	86
P10-2 200°C	66

Table 4 shows the total fibre count on the specimen surfaces at different temperatures. At the maximum test temperature, many fibres disappeared, preventing an accurate determination of the fibre orientation coefficient. Figure 11 illustrates the fibre orientation coefficient after exposure to high temperatures, highlighting the impact of heat on fibre distribution.

Figure 11 summarizes the orientation coefficients. At 20°C, P10 specimens had a coefficient of 0.47, lower than expected for self-compacting concrete [23, 24]. At 165°C, the orientation factor aligned with expected values [25, 26], but at 185°C, a decrease was

observed, possibly due to manufacturing conditions or fibre melting.

At 200°C, a clear correlation between the orientation factor and the mechanical response was found. The absence of a reloading stage suggests a reduction in fibre presence on the fracture surface, likely due to complete fibre melting. While this negatively impacts mechanical performance, it could help reduce internal pressure at high temperatures, potentially preventing spalling, a phenomenon that warrants further study.

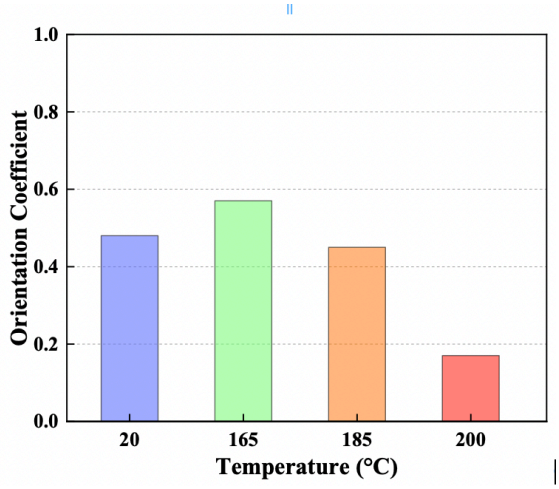

Figure 11. Results of the orientation coefficient calculations for HRFP.

5 CONCLUSIONS

This study evaluates the effect of high temperatures on the fracture performance of PFRC according to EN 14651:2007, comparing its behavior at 20°C, 165°C, 185°C, and 200°C. The temperature range was selected based on the 164°C melting point of the fibres. A thermal insulation system limited heat loss to 0.44°C/min, ensuring the material's behavior was accurately assessed at the target temperature.

Temperature gradually altered the mechanical response, but the variation was non-linear, becoming abrupt once the fibre melting point was exceeded. At 20°C, P10 exhibited structural PFRC behavior, while at 165°C and 185°C, it retained some ductility. However, at 200°C, the material behaved almost like plain concrete.

The contribution of the fibres in the structural design could be considered according to MC2010 [6] at 165º if the material was designed for being constantly at such temperature. However, if heated to 165°C after being designed for room temperature, it did not meet f_{R1} requirements. For temperatures above 165°C, fibre contribution should not be considered in the design. Since high-temperature structural design is not covered in current standards, residual strengths at each temperature should be evaluated.

The strength at the limit of proportionality decreased by 40%, while f_{R1} dropped by 42%, with f_{R3} experiencing the highest reduction of 66%, approximately. Since f_{R3} is typically used for Ultimate Limit States, this drop is critical.

It meets structural requirements if PFRC is heated to 165°C and then tested at room temperature. However, when tested at 165°C, it does not fully comply. For temperatures above 165°C, the material fails to meet structural requirements, regardless of when the test is performed. At room temperature, fibres contribute structurally due to their surface roughness. As temperature increases, fibres soften, and by 185°C, they retain some structural character, but at 200°C, they undergo a state change, causing the material to behave similarly to non-fibre-reinforced concrete.

A future research focus will be on the roughness of fibres after flexural tensile tests, as this could further explain their structural contribution loss at high temperatures.

5 ACKNOWLEDGEMENTS

The authors gratefully acknowledge the financial support provided by Ministry of Science and Innovation of Spain by means of the Research Fund Project PID2023-149321OB-C31 and TED2021-130734B-I00. They also offer their gratitude to SIKA SAU for supplying the polyolefin fibres.

REFERENCES

[1] F. Carrasco, S. Grathwohl, J. Maier, J. Ruppert, G. Scheffknecht, Experimental investigations of oxyfuel burner for cement production application, *Fuel* 236 (2019)

608–614. https://doi.org/10.1016/j.fuel.2018.08.135.

[2] E. De Lena, M. Spinelli, I. Martínez, M. Gatti, R. Scaccabarozzi, G. Cinti, M.C. Romano, Process integration study of tail-end Ca-Looping process for CO2 capture in cement plants, *International Journal of Greenhouse Gas Control* 67 (2017) 71–92. https://doi.org/10.1016/j.ijggc.2017.10.005.

[3] M. Schneider, The cement industry on the way to a low-carbon future, Cem Concr Res 124 (2019). https://doi.org/10.1016/j.cemconres.2019.105792.

[4] E.S. Bernard, A.H. Thomas, Fibre reinforced sprayed concrete for ground support, Tunnelling and Underground Space Technology 99 (2020). https://doi.org/10.1016/j.tust.2020.103302.

[5] A.R.E. Cáceres, S.H.P. Cavalaro, A.D. de Figueiredo, Integrated approach for quality control of fibre-reinforced sprayed concrete for tunnel lining, Tunnelling and Underground Space Technology 140 (2023). https://doi.org/10.1016/j.tust.2023.105260.

[6] M. Namli, Evaluation of the effect of using fiber reinforcement in tunnel linings for metro projects, Underground Space (China) 6 (2021) 732–750. https://doi.org/10.1016/j.undsp.2021.08.002.

[7] M. Khooshechin, J. Tanzadeh, Experimental and mechanical performance of shotcrete made with nanomaterials and fiber reinforcement, Constr Build Mater 165 (2018) 199–205. https://doi.org/10.1016/j.conbuildmat.2017.12.199.

[8] A. Conforti, G. Tiberti, G.A. Plizzari, A. Caratelli, A. Meda, Precast tunnel segments reinforced by macro-synthetic fibers, Tunnelling and Underground Space Technology 63 (2017) 1–11. https://doi.org/10.1016/j.tust.2016.12.005.

[10] M. Mazloom, S. Mirzamohammadi, Fracture of fibre-reinforced cementitious composites after exposure to elevated temperatures, *Magazine of Concrete Research* 73 (2021) 701–713. https://doi.org/10.1680/jmacr.19.00401.

[11] G.F. Peng, W.W. Yang, J. Zhao, Y.F. Liu, S.H. Bian, L.H. Zhao, Explosive spalling and residual mechanical properties of fiber-toughened high-performance concrete subjected to high temperatures, *Cem Concr Res* 36 (2006) 723–727. https://doi.org/10.1016/j.cemconres.2005.12.014.

[12] Y. Ding, C. Azevedo, J.B. Aguiar, S. Jalali, Study on residual behavior and flexural toughness of fiber cocktail reinforced self-compacting high-performance concrete after exposure to high temperature, *Constr Build Mater* 26 (2012) 21–31. https://doi.org/10.1016/j.conbuildmat.2011.04.058.

[13] K. Watanabe, M.R. Bangi, T. Horiguchi, The effect of testing conditions (hot and residual) on fracture toughness of fiber reinforced high-strength concrete subjected to high temperatures, *Cem Concr Res* 51 (2013) 6–13. https://doi.org/10.1016/j.cemconres.2013.04.003.

[14] M.G. Alberti, J.C. Gálvez, A. Enfedaque, R. Castellanos, Influence of high temperature on the fracture properties of polyolefin fibre reinforced concrete, *Materials* 14 (2021) 1–21. https://doi.org/10.3390/ma14030601.

[15] European Committee for Standardization, Test Method for Metallic Fiber Concrete. Measuring the Flexural Tensile Strength (Limit of Proportionality (LOP), Residual), *EN14651:2007+A1, 2007*.

[16] European Committee for Standardization, Fibers for Concrete. Polymer Fibers. Definitions, Specifications and Conformity, *EN 14889-2, 2008*.

[17] International Federation for Structural Concrete (fib), *The fib Model Code for Concrete Structures 2010*. Lausanne, Switzerland: International Federation for Structural Concrete, 2010.

[18] O. Smirnova, A. Kharitonov, Y. Belentsov, Influence of polyolefin fibers on road

pavement concrete's strength and deformability properties, *Journal of Traffic and Transportation Engineering* (English Edition) 6 (2019) 407–417. https://doi.org/10.1016/j.jtte.2017.12.004.

[19] M.G. Alberti, A. Enfedaque, J.C. Gálvez, Comparison between polyolefin fibre reinforced vibrated conventional concrete and self-compacting concrete, *Constr Build Mater* 85 (2015) 182–194. https://doi.org/10.1016/j.conbuildmat.2015.03.007.

[20] M.G. Alberti, A. Enfedaque, J.C. Gálvez, On the prediction of the orientation factor and fibre distribution of steel and macro-synthetic fibres for fibre-reinforced concrete, Cem Concr Compos 77 (2017) 29–48. https://doi.org/10.1016/j.cemconcomp.2016.11.008.

[21] C. Maluk, J. Tignard, A. Ridout, T. Clarke, R. Winterberg, Experimental study on the fire behaviour of fibre reinforced concrete used in tunnel applications, *Fire Saf J* 120 (2021). https://doi.org/10.1016/j.firesaf.2020.103173.

[22] M.G. Alberti, J.C. Gálvez, A. Enfedaque, R. Castellanos, Influence of high temperature on the fracture properties of polyolefin fibre reinforced concrete, *Materials* 14 (2021) 1–21. https://doi.org/10.3390/ma14030601.

[23] M.G. Alberti, A. Enfedaque, J.C. Gálvez, E. Reyes, Numerical modelling of the fracture of polyolefin fibre reinforced concrete by using a cohesive fracture approach, *Compos B Eng* 111 (2017) 200–210. https://doi.org/10.1016/j.compositesb.2016.11.052.

[24] R.A. Raju, S. Lim, M. Akiyama, T. Kageyama, Effects of concrete flow on the distribution and orientation of fibers and flexural behavior of steel fiber-reinforced self-compacting concrete beams, Constr Build Mater 262 (2020). https://doi.org/10.1016/j.conbuildmat.2020.119963.

[25] E. V. Sarmiento, M.R. Geiker, T. Kanstad, Influence of fibre distribution and orientation on the flexural behaviour of beams cast from flowable hybrid polymer-steel FRC, *Constr Build Mater* 109 (2016) 166–176. https://doi.org/10.1016/j.conbuildmat.2016.02.005.

[26] M.G. Alberti, A. Enfedaque, J.C. Gálvez, V. Agrawal, Fibre distribution and orientation of macro-synthetic polyolefin fibre reinforced concrete elements, *Constr Build Mater* 122 (2016) 505–517. https://doi.org/10.1016/j.conbuildmat.2016.06.083.